Electronic Supplementary Material (ESI) for Physical Chemistry Chemical Physics.

Supplementary Information
Optical lateral forces and torques induced by chiral surface-plasmon-polaritons and their potential applications in recognition and separation of chiral enantiomers

Qiang Zhang, *JunqingLi** and Xingguang Liu
Department of Physics, Harbin Institute of Technology, 92 Western Dazhi, Harbin 150001, China.
E-mail: jqli@hit.edu.cn

1 Implementation of constitutive relations for chiral materials in COMSOL

For bi-isotropic materials, the electric displacement **D** and magnetic induction **B** are related to the electric (**E**) and magnetic (**H**) field as follows:

$$\mathbf{D} = \varepsilon_0 \varepsilon_c \mathbf{E} - i\xi \mathbf{B} \qquad (1)$$
$$\mathbf{H} = \mathbf{B}/\mu_c - i\xi \mathbf{E},$$

or

$$\mathbf{D} = \varepsilon_0 \varepsilon_c \mathbf{E} - i\kappa/c\mathbf{H} \qquad (2)$$
$$\mathbf{B} = \mu_c \mu_0 \mathbf{H} + i\kappa/c\mathbf{E},$$

where ε_c, μ_c and ξ are the relative permittivity, relative permeability and chirality of the chiral medium, respectively, and $\kappa = \xi \mu_0 c$. The chiral constitutive equations have been implemented within COMSOL Multiphysics, which solves Maxwell's equations using a finite element method. The modifications are applied to the Wave Optics Module, Electromagnetic Waves, Frequency Domain, which are adopted by many works[1–4].

The equation for **D** components is modified as

ewfd.Dx: epsilon0_const*ewfd.Ex+ewfd.Px-i*kappa/c0_const*ewfd.Hx
ewfd.Dy: epsilon0_const*ewfd.Ey+ewfd.Py-i*kappa/c0_const*ewfd.Hy
ewfd.Dz: epsilon0_const*ewfd.Ez+ewfd.Pz-i*kappa/c0_const*ewfd.Hz

The equation for **H** components is modified as

ewfd.Hx: (ewfd.murinvxx*(ewfd.Bx-i*kappa/_const*ewfd.Ex)+
ewfd.murinvxy*(ewfd.By-i*kappa/c0_const*ewfd.Ey)+
ewfd.murinvxz*(ewfd.Bz-i*kappa/c0_const*ewfd.Ez))/mu0_const
ewfd.Hy: (ewfd.murinvyx*(ewfd.Bx-i*kappa/c0*ewfd.Ex)+
ewfd.murinvyy*(ewfd.By-i*kappa/c0_const*ewfd.Ey)+
ewfd.murinvyz*(ewfd.Bz-i*kappa/c0_const*ewfd.Ez))/mu0_const
ewfd.Hz: (ewfd.murinvzx*(ewfd.Bx-i*kappa/c0*ewfd.Ex)+
ewfd.murinvzy*(ewfd.By-i*kappa/c0_const*ewfd.Ey)+
ewfd.murinvzz*(ewfd.Bz-i*kappa/c0_const*ewfd.Ez))/mu0_const

The equation for $\mathbf{dH}/\mathbf{dt}$ components is modified as

ewfd.dHdtx: (ewfd.murinvxx*(ewfd.dBdtx-i*kappa/c0_const*ewfd.iomega*ewfd.Ex)+
ewfd.murinvxy*(ewfd.dBdty-i*kappa/c0_const*ewfd.iomega*ewfd.Ey)+

ewfd.murinvxz*(ewfd.dBdtz-i*kappa/c0_const*ewfd.iomega*ewfd.Ez))/mu0_const
ewfd.dHdty: (ewfd.murinvyx*(ewfd.dBdtx-i*kappa/c0_const*ewfd.iomega*ewfd.Ex)+
ewfd.murinvyy*(ewfd.dBdty-i*kappa/c0_const*ewfd.iomega*ewfd.Ey)+
ewfd.murinvyz*(ewfd.dBdtz-i*kappa/c0_const*ewfd.iomega*ewfd.Ez))/mu0_const
ewfd.dHdtz: (ewfd.murinvzx*(ewfd.dBdtx-i*kappa/c0_const*ewfd.iomega*ewfd.Ex)+
ewfd.murinvzy*(ewfd.dBdty-i*kappa/c0_const*ewfd.iomega*ewfd.Ey)+
ewfd.murinvzz*(ewfd.dBdtz-i*kappa/c0_const*ewfd.iomega*ewfd.Ez))/mu0_const

2 Simulation of the reflection spectra, optical forces and torques in COMSOL

For the calculation of reflection spectra, we build a 3D model. The model has perfectly matched layers (PMLs) on the top and bottom of the model, where in between them are three blocks whose heights are H1=800nm, t=45nm and H2=800nm, corresponding to the prism (n=1.766), gold and the chiral environment, respectively. Port 1 at the interface between the top PML and prism is set as circularly polarized light (CPL) on, while Port 2 at the interface between the bottom PML and the chiral environment is set as CPL off. The out side of the PMLs are set with Scattering Boundary Conditions (SBCs). To calculate the reflection spectra of a light illuminating on a smooth metal surface, the width of the 3D block should be very much shorter than the wavelength of interest, thus here is 30nm, which is $< 1/20\lambda$. The maximum size of the grid is 10nm, $< 1/60\lambda$, and the number of degrees of freedom is 0.32 million. We should note here that for CPL illumination, Port 2 can not be used to detect the reflection spectra because the reflected waves are not CPL any more. An additional surface should be added to the vicinity of Port 1, thereby the accurate reflection spectra can be calculated by the surface integration of the Poynting vector, as shown in Fig. 1.

Then we tested the simulation convergence by changing the height of both the prism and chiral environment in the model, and the results show good convergence for different heights, as shown in Fig. 2 to 6.

The most accurate results of the calculation of optical lateral force and optical torques in the scattering problem should be obtained from 3D full wave simulation in COMSOL. However, the mesh should be extremely fine enough to be convincing which relies on an extremely huge amount of computer memory that goes up to over 300 G. Fortunately, according to the dipole approximation, when the radius of the nano-particle is very much smaller than the wavelength of inter-

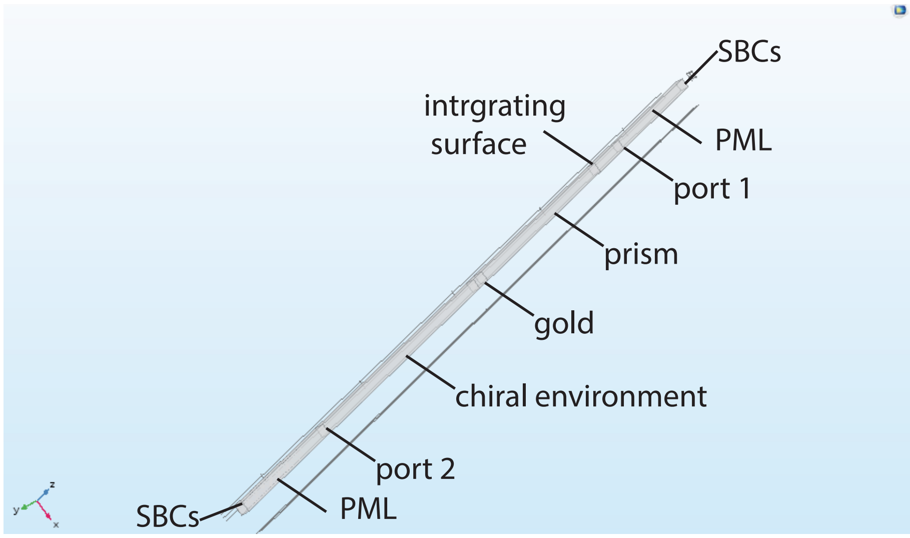

Figure 1: 3D model for calculating the reflection spectra.

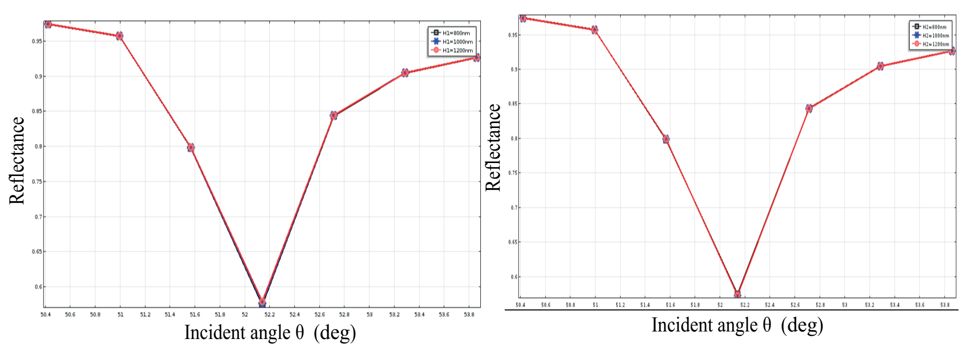

Figure 2: Validation of convergence by changing H1(left) and H2(right), when $\xi = -0.5 \times 10^{-4}$.

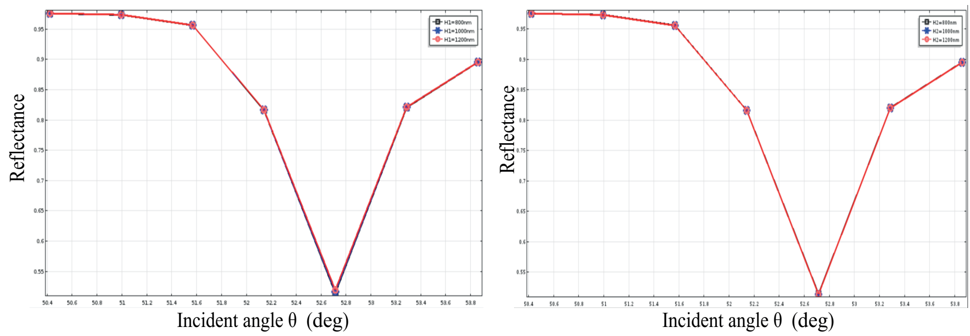

Figure 3: Validation of convergence by changing H1(left) and H2(right), when $\xi = -0.2 \times 10^{-4}$.

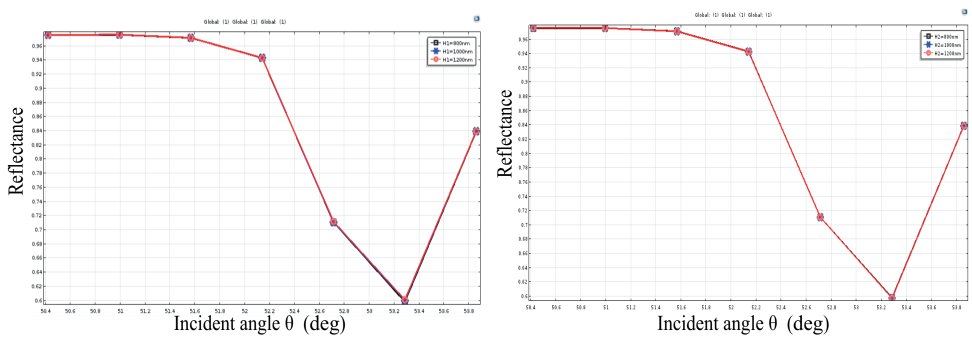

Figure 4: Validation of convergence by changing H1(left) and H2(right), when $\xi = 0$.

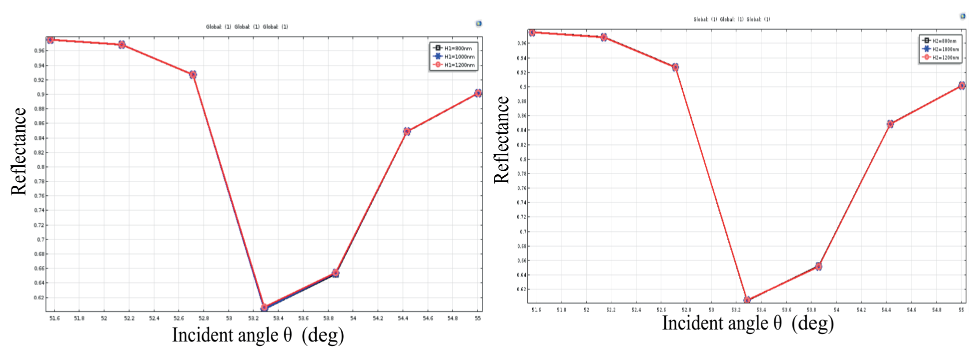

Figure 5: Validation of convergence by changing H1(left) and H2(right), when $\xi = +0.2 \times 10^{-4}$.

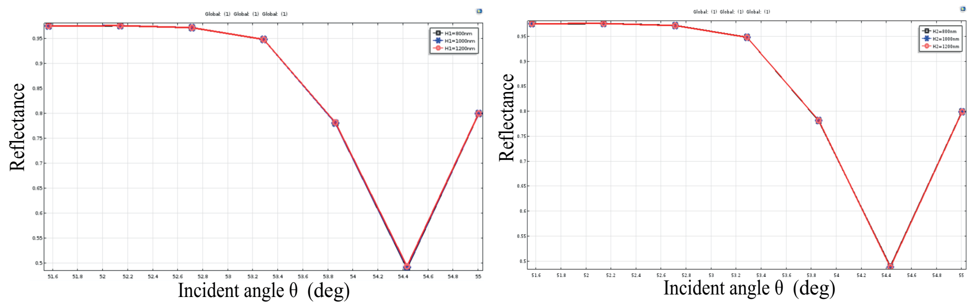

Figure 6: Validation of convergence by changing H1(left) and H2(right), when $\xi = +0.5 \times 10^{-4}$.

est, it is sufficient to simplify the problem to 2D[3,5]. In the 2D model simulating the scattering problem of the chiral nano-particle, the maximum size of the grid for the prism is 18nm, $< 1/30\lambda$, the maximum size of the grid for the gold film is 5nm, the maximum size of the grid for the chiral nano-particle sphere is 2nm which is $< 1/300\lambda$, and the number of degrees of freedom is 1.73 million with its corresponding required computer memory being 22 G.

3 References

(1) The Role of Plasmon-Generated Near Fields for Enhanced Circular Dichroism Spectroscopy, Maxim L. Nesterov, Xinghui Yin, Martin Schäferling, Harald Giessen, and Thomas Weiss, ACS Photonics, 2016, 3 (4), pp 578-583.
(2) Controlling Metamaterial Transparency with Superchiral Fields, Christopher Kelly, Larousse Khosravi Khorashad, Nikolaj Gadegaard, Laurence D. Barron, Alexander O. Govorov, Affar S. Karimullah, and Malcolm Kadodwala, ACS Photonics, 2018, 5 (2), pp 535-543.
(3) All-Optical Chirality-Sensitive Sorting via Reversible Lateral Forces in Interference Fields, Tianhang Zhang, Mahdy Rahman Chowdhury Mahdy, Yongmin Liu, Jing Hua Teng, Chwee Teck Lim, Zheng Wang, and Cheng-Wei Qiu, ACS Nano, 2017, 11 (4), pp 4292-4300.
(4) Helicity Preserving and Resonant Structures for Enhanced Chiral Molecule Detection, Florian Graf, Carsten Rockstuhl, Ivan Fernandez-Corbaton, arXiv:1810.08385, 2018.
(5) Lateral optical force on chiral particles near a surface, S. B. Wang and C. T. Chan, Nat. Commun., 2014, 5, 3307.